

Article

Synthesis and Characterization of SiO₂/TiO₂ as Photocatalyst on Methylene Blue Degradation

Aleksandra Babyszko, Agnieszka Wanag *, Marcin Sadłowski, Ewelina Kusiak-Nejman 
and Antoni W. Morawski 

Faculty of Chemical Technology and Engineering, Department of Inorganic Chemical Technology and Environment Engineering, West Pomeranian University of Technology in Szczecin, Pułaskiego 10, 70-322 Szczecin, Poland

* Correspondence: awanag@zut.edu.pl

Abstract: The paper presents a modification of titanium dioxide with fumed silica. The SiO₂/TiO₂ photocatalysts were obtained by the sol-gel method and then were calcined under an argon atmosphere. Various SiO₂ weights (2–17.2 wt.%) were used in the materials' preparation stage. The obtained samples were characterized using advanced analytical methods, such as FT-IR/DRS infrared spectroscopy, X-ray diffraction, SEM scanning electron microscopy, and UV-Vis/DRS spectroscopy. The BET specific surface area and zeta potential of samples were also measured. Based on the obtained results, it was observed that the modification of titanium dioxide with SiO₂ effectively inhibited the increase in crystallite size of anatase and brookite during calcination and the decrease in specific surface area values. Moreover, the presence of SiO₂ in the nanomaterials contributed to the increase in the size of specific surface area and the change in band gap energy values. The photocatalytic activity was determined based on the decomposition of methylene blue under UV irradiation. Thermal modification in an inert gas atmosphere significantly increased the dye removal rate. It should be noted that all the obtained SiO₂/TiO₂ photocatalysts showed higher activity compared to the starting TiO₂. It was also found that the photocatalytic activity increased along with the increase in SiO₂ content in the sample (up to 14.3 wt.% of SiO₂). The highest activity was recorded for SiO₂(11.1%)/TiO_{2_400} and SiO₂(14.3%)/TiO_{2_400} samples.

Keywords: photocatalysis; titanium dioxide; fumed silica; methylene blue decomposition



Citation: Babyszko, A.; Wanag, A.; Sadłowski, M.; Kusiak-Nejman, E.; Morawski, A.W. Synthesis and Characterization of SiO₂/TiO₂ as Photocatalyst on Methylene Blue Degradation. *Catalysts* **2022**, *12*, 1372. <https://doi.org/10.3390/catal12111372>

Academic Editors: Jorge Bedia, Carolina Belver and Gassan Hodaifa

Received: 30 September 2022

Accepted: 3 November 2022

Published: 5 November 2022

Publisher's Note: MDPI stays neutral with regard to jurisdictional claims in published maps and institutional affiliations.



Copyright: © 2022 by the authors. Licensee MDPI, Basel, Switzerland. This article is an open access article distributed under the terms and conditions of the Creative Commons Attribution (CC BY) license (<https://creativecommons.org/licenses/by/4.0/>).

1. Introduction

Advanced oxidation processes are promising methods for removing pollutants from the environment. One is heterogeneous photocatalysis, which can purify water and air [1–4]. Due to its properties, titanium dioxide is one of the most commonly used semiconductors in the photocatalytic oxidation of organic compounds. It is characterized by a relatively low price, non-toxicity, high photoactivity, and chemical stability [5]. At the same time, intensive research is being conducted worldwide to increase the efficiency of photocatalytic processes. The studies aim to improve the physicochemical properties of titanium dioxide affecting photocatalytic activity.

There are many methods used to obtain TiO₂, such as hydrothermal, solvothermal, sol-gel, or precipitation [6], but the sol-gel method is effective for controlling the size and morphology of the synthesized particles while obtaining homogeneous materials [7–11]. During the sol-gel process, factors such as the initial composition of the reaction mixture, i.e., the molar ratio of water to the metal precursor, type of solvent, type and concentration of catalyst, temperature, and the pH of the solution affect the rate of hydrolysis and polycondensation [12]. In addition, calcination also significantly influences the physical and chemical properties of the final product [13]. For example, Ciesielczyk et al. [14] proved that calcination causes significant changes in the porous structure parameters. In

particular, there was a significant reduction in the surface area and pore volume for the calcined samples.

Photocatalysts with enhanced activity can be obtained by modifying titanium dioxide using various compounds, e.g., metals or their oxides and non-metals [15]. Recently, the silica modification of titanium dioxide is becoming more popular. It has been proven that the addition of SiO₂ increases the surface of the photocatalyst, increasing the adsorption of pollutants [16]. The enhanced adsorption of contaminants on the silica surface, in turn, improves the photocatalytic activity of mixed SiO₂–TiO₂ oxides compared to pure TiO₂ [17,18]. Jimmy et al. [19] and Yu et al. [20] found that the addition of SiO₂ causes the inhibition of TiO₂ crystallization. Moreover, adding SiO₂ increases the amount of water and hydroxyl groups adsorbed on the surface, improving the hydrophilic and photocatalytic properties [21–23].

Several methods of preparation of TiO₂ with silica are presented in the literature. The most commonly used silica precursors are tetraethoxysilane (TEOS), tetramethoxysilane (TMOS), and silica gel [24,25]. The sol-gel method for the synthesis of TiO₂/SiO₂ was used by Fatimah [24]. Titanium(IV) isopropoxide (TTIP) was used as a TiO₂ precursor, while tetramethoxysilane (TMOS) and tetraethoxysilane (TEOS) were used as silica precursors. The molar ratio of titanium dioxide to silicon was 4:9. The obtained nanomaterials were then calcined at 500 °C for 4 h. The photocatalytic activity of new nanomaterials was determined based on the decomposition of methylene blue. It was found that using tetraethoxysilane as a silica precursor results in obtaining material with a larger specific surface area and pore volume, which in turn increases photocatalytic efficiency. Qourzal et al. [25] obtained a TiO₂-SiO₂ photocatalyst by hydrolyzing TTIP in silica gel. The material was calcined at 400 °C for 2 h in the air atmosphere. It was noted that the presence of silica suppresses the anatase to rutile phase transformation. Based on the decomposition of β-naphthol under UV light, they found that the prepared material showed 2.7, 4, and 7.8 times higher photocatalytic activity than commercial TiO₂ P25, TiO₂ PC50, and TiO₂ “Aldrich” photocatalysts, respectively. Enhanced photocatalytic activity has been attributed to the high adsorption capacity of the photocatalyst and a large specific surface area. Nandanwar et al. [26] obtained composites by the sol-gel method, using titanium(IV) isopropoxide as TiO₂ precursor, tetraethoxysilane (TEOS) as silica precursor, ethanol as solvent, and hydrochloric acid as a promoter of the hydrolysis reaction. In addition, polyethylene glycol (PEG) and the non-ionic Triton X-100 surfactant were used during the preparation phase. The photocatalytic activity was measured by methylene blue degradation. In the case of the Triton X-100 sample, after only a few minutes of exposure to the UV light, approx. 50% of methylene blue was degraded. These results confirm that TiO₂/SiO₂ with the addition of Triton X-100 shows a higher degradation efficiency than TiO₂/SiO₂ with polyethylene glycol.

This work proposes a new method of titanium dioxide nanomaterial modification with fumed silica. SiO₂/TiO₂ nanomaterials were prepared using the sol-gel method. An essential element of the preparation was introducing the heating stage of the obtained nanomaterials in the argon atmosphere. This represents a kind of novelty concerning the preparation methods because, in the methods described in the literature for obtaining this type of materials, the calcination process was carried out mainly in an air atmosphere. The photocatalytic activity of gained samples was determined based on the methylene blue decomposition under UV irradiation. The effect of specific physicochemical properties on photocatalytic activity was also investigated. To the best of our knowledge, this is the first paper in which fumed silica with average primary particle size of 7–14 nm was used as a silica precursor. According to the manufacturer, the used silica characterizes a relatively large specific surface area (>200 m²/g). The novelty of the presented study was also the determination of the calcination effect on the photocatalytic and physicochemical properties of TiO₂ nanomaterials modified with fumed silica obtained in an inert gas atmosphere.

2. Results and Discussion

2.1. Characterization of the Photocatalysts

The surface character of the prepared TiO₂ samples was analysed by FT-IR/DRS spectroscopy. In Figure 1A,B, the FT-IR/DR spectra of starting TiO₂, silica-modified TiO₂ and samples calcined in an argon atmosphere are shown. All spectra presented characteristic bands for TiO₂-based nanomaterials. Analysing the obtained spectra, the bands in the range of 3730–2500 cm⁻¹ attributed to the stretching mode of O–H group were confirmed [27]. As can be seen from Figure 1A,B, the intensity of the mentioned peaks increased with the increasing amount of silica used for modification. It was related to the presence of Si–OH groups and adsorbed water formed by silica deposition on titanium particles [28]. After the calcination process (see Figure 1B), a decrease in the intensity of this band was observed compared to the unheated materials due to the change in the content of hydroxyl groups on the semiconductor surface [29]. The narrow band located at 1610 cm⁻¹ is characteristic of the vibrations of molecular water bending mode [30]. Band located at 3710 cm⁻¹ corresponds to the OH groups surface-bonded to titanium [31,32]. At 930 cm⁻¹, an intense band assigned to the O–Ti–O stretching modes was observed, and for photocatalysts modified with silica, the band in question was slightly shifted, which indicates the presence of interaction between titanium and silicon [33]. After silica modification, a new band located at 1160 cm⁻¹ attributed to the asymmetrical stretching of Si–O–Si bonds was noticed [34]. It can be noted that the intensity of the upper-mentioned peak increased with the increase in silica amount used for TiO₂ modification. The peak noticed at 1780 cm⁻¹ was ascribed to the C=O stretching vibration.

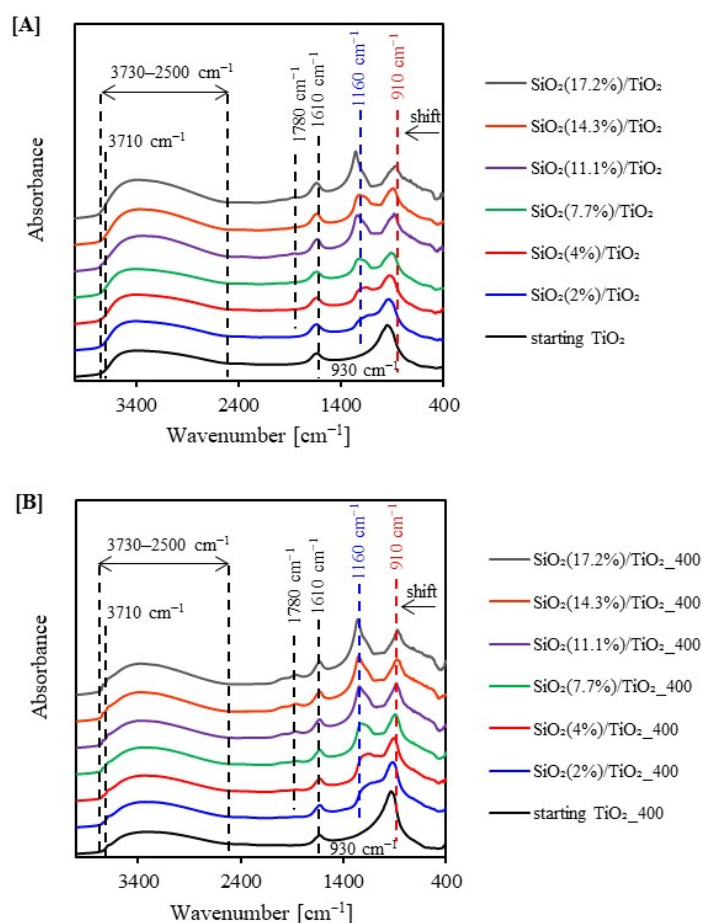


Figure 1. FT-IR/DR spectra of starting TiO₂ and silica-modified TiO₂ prior (A) and after heat treatment (B).

In Figure 2A,B, the XRD diffraction patterns of the starting TiO_2 , silica-modified TiO_2 and samples calcined in an argon atmosphere are shown. The phase composition and average crystallite sizes of the studied samples are compared in Table 1. It should be noted that the presented results refer to the crystalline phase. Based on the analysis of obtained data, the presence of reflections characteristic of anatase and brookite was found. The characteristic reflections (101), (004), (200), (105), (204), (116), and (215), corresponding to the anatase phase, were recorded at $2\theta = 25.6, 38.6, 48.8, 55.2, 63.6, 70.1,$ and 76.3° , respectively (JCPDS 04-002-8296 PDF4+ card). Two reflections (111), (121) characteristic of the brookite phase were recorded at $2\theta = 25.6$ and 30.3° (JCPDS 04-007-0758 PDF4+ card). The reflection from brookite located at $2\theta = 25.6^\circ$ overlapped with the reflection characteristic of anatase. Therefore, the size of brookite crystallites was calculated based on the reflectance located at $2\theta = 30.3^\circ$. The presence of the brookite phase was due to the use of hydrochloric acid as a catalyst for the hydrolysis reaction of titanium(IV) isopropoxide [35]. It can be noted that calcination at 400°C did not contribute to the phase transition of anatase to rutile, and this is a typical phenomenon because the phase transition of anatase to rutile occurs at temperatures above 600°C [36]. It is also worth noting that the reflections narrowed and sharpened after calcination. This was attributed to eliminating defects at grain boundaries during heating at higher temperatures [37]. According to the data in Table 1, the anatase to brookite ratio remained similar, i.e., 59:41, only when the amount of silica precursor introduced was 11.1wt.% the anatase content started to increase. This can be explained by the fact that the amorphous phase was not included in the presented results. As it is known, silica used for modification was amorphous. Therefore, the observed increase in the anatase phase with increasing SiO_2 content may be overestimated by up to 20–30%. After the calcination process, a decrease in brookite content was observed, which was related to the greater crystallization of anatase than brookite. Only when the amount of silica precursor introduced was 11.1wt.% the brookite content start increasing, which was related to the crystallization process progress. It should also be noted that the calcination process had a significant effect on the increase in average anatase and brookite crystallite size. The average crystallite sizes of anatase for non-calcined materials were 4–5 nm and 8–16 nm for the calcined samples. In contrast, the crystallite sizes of brookite ranged from 2 to 6 nm for non-calcined photocatalysts and 7–9 nm for calcined photocatalysts. This indicates an increase in the crystallinity of samples after calcination. However, comparing the crystallite size of $\text{SiO}_2/\text{TiO}_2$ materials after heating with starting TiO_2_{400} sample, it can be observed that the crystallite size of anatase and brookite was smaller for silica-modified photocatalysts than for the sample without SiO_2 addition. For example, the size of anatase crystallites for starting TiO_2_{400} was 14 nm, while for the $\text{SiO}_2(17.2\%)/\text{TiO}_2_{400}$ sample, it was only 8 nm. According to Xu et al. [38] and Lu et al. [39], silica can effectively prevent the growth of TiO_2 crystallites during the calcination process.

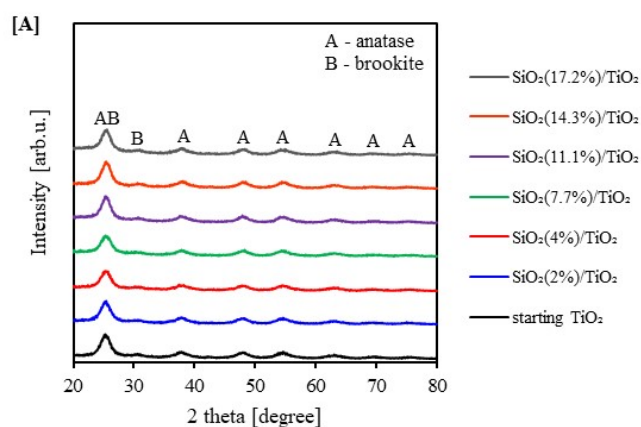


Figure 2. Cont.

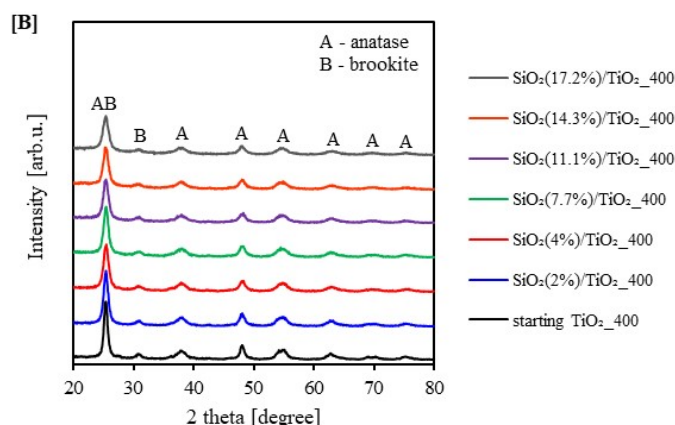


Figure 2. XRD patterns of starting TiO₂ and silica-modified TiO₂ prior (A) and after heat treatment (B).

Table 1. XRD phase composition, average crystallites size, specific surface area and pore volume distribution of starting TiO₂ and silica-modified photocatalysts.

| Sample Code | Phase Composition [%] | | Mean Crystallite Size [nm] | | S _{BET} [m ² /g] | V _{total} [cm ³ /g] | V _{micro} [cm ³ /g] | V _{meso} [cm ³ /g] |
|---|-----------------------|----------|----------------------------|----------|--------------------------------------|---|---|--|
| | Anatase | Brookite | Anatase | Brookite | | | | |
| starting TiO ₂ | 57 | 43 | 5 ± 0.2 | 2 ± 0.2 | 193 | 0.109 | 0.079 | 0.030 |
| SiO ₂ (2%)/TiO ₂ | 58 | 42 | 5 ± 0.2 | 2 ± 0.2 | 234 | 0.159 | 0.090 | 0.069 |
| SiO ₂ (4%)/TiO ₂ | 59 | 41 | 5 ± 0.2 | 4 ± 0.2 | 221 | 0.148 | 0.090 | 0.058 |
| SiO ₂ (7.7%)/TiO ₂ | 59 | 41 | 5 ± 0.2 | 4 ± 0.2 | 218 | 0.171 | 0.085 | 0.171 |
| SiO ₂ (11.1%)/TiO ₂ | 81 | 19 | 5 ± 0.2 | 5 ± 0.2 | 208 | 0.265 | 0.080 | 0.185 |
| SiO ₂ (14.3%)/TiO ₂ | 77 | 23 | 5 ± 0.2 | 6 ± 0.2 | 207 | 0.285 | 0.080 | 0.205 |
| SiO ₂ (17.2%)/TiO ₂ | 81 | 19 | 4 ± 0.2 | 6 ± 0.2 | 228 | 0.366 | 0.088 | 0.278 |
| starting TiO _{2_400} | 63 | 37 | 14 ± 0.4 | 9 ± 0.4 | 54 | 0.101 | 0.020 | 0.081 |
| SiO ₂ (2%)/TiO _{2_400} | 66 | 34 | 16 ± 0.4 | 7 ± 0.4 | 89 | 0.177 | 0.031 | 0.146 |
| SiO ₂ (4%)/TiO _{2_400} | 68 | 32 | 11 ± 0.4 | 7 ± 0.4 | 98 | 0.160 | 0.036 | 0.124 |
| SiO ₂ (7.7%)/TiO _{2_400} | 66 | 34 | 11 ± 0.4 | 7 ± 0.4 | 104 | 0.189 | 0.039 | 0.150 |
| SiO ₂ (11.1%)/TiO _{2_400} | 67 | 33 | 10 ± 0.4 | 7 ± 0.4 | 121 | 0.259 | 0.043 | 0.216 |
| SiO ₂ (14.3%)/TiO _{2_400} | 72 | 28 | 9 ± 0.4 | 8 ± 0.4 | 135 | 0.313 | 0.051 | 0.262 |
| SiO ₂ (17.2%)/TiO _{2_400} | 72 | 28 | 8 ± 0.4 | 8 ± 0.4 | 146 | 0.371 | 0.056 | 0.315 |

The adsorption–desorption N₂ isotherms of starting TiO₂ and the SiO₂/TiO₂ materials are shown in Figures 3 and 4. It can be noted that the samples presented three kinds of isotherm types. Most of the photocatalysts (starting TiO₂, SiO₂(2, 4%)/TiO₂, starting TiO_{2_400}, SiO₂(2–7.7%)/TiO_{2_400}) displayed a typical type IV isotherm with an H3 hysteresis loop, which is characteristic of mesoporous materials, according to the IUPAC classification [40]. The H3-type hysteresis loop does not show any adsorption limit in the high relative pressure range and is characteristic of slotted pores [41,42]. The sample (starting TiO₂) showed a type I isotherm characteristic of microporous materials. On the other hand, SiO₂(2%)/TiO₂ and SiO₂(4%)/TiO₂ isotherms in the initial p/p₀ range were defined as type I isotherm, and in the intermediate and higher pressure range as type II isotherm. The isotherms of starting TiO_{2_400}, SiO₂(2%)/TiO_{2_400}, SiO₂(4%)/TiO_{2_400} and SiO₂(7.7%)/TiO_{2_400} samples demonstrated an asymmetric and triangular type H2 of the hysteresis loop, what was attributed to blockage of pores/percolation in a narrow range of pore necks [40,43]. For starting TiO₂, the hysteresis loop did not occur.

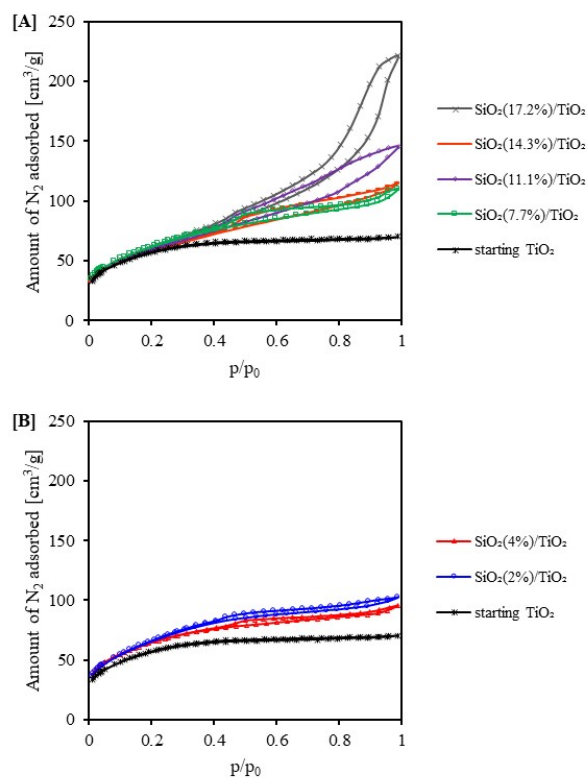


Figure 3. Adsorption–desorption isotherms of: (A) starting TiO₂, SiO₂(2%)/TiO₂ and SiO₂(4%)/TiO₂, (B) starting TiO₂, SiO₂(7.7%)/TiO₂, SiO₂(11.1%)/TiO₂, SiO₂(14.3%)/TiO₂ and SiO₂(17.2%)/TiO₂.

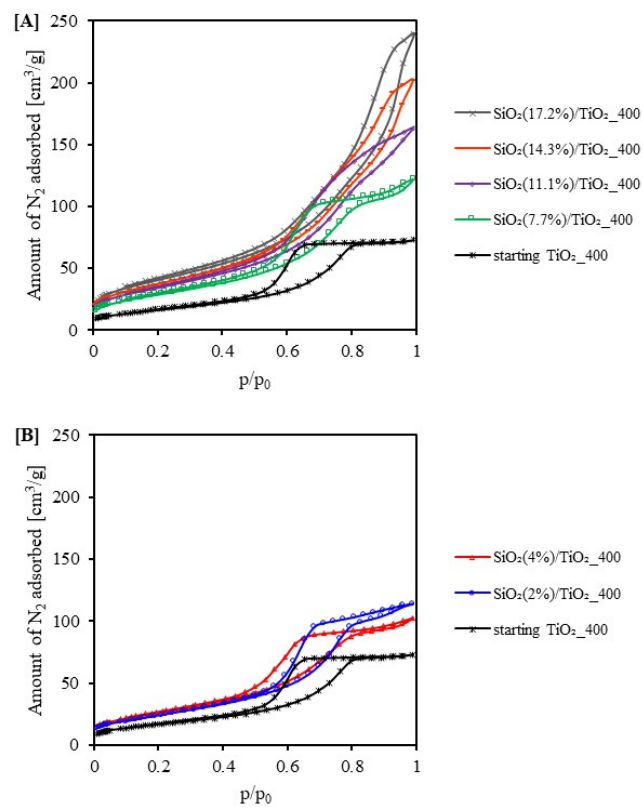


Figure 4. Adsorption–desorption isotherms of: (A) starting TiO_{2_400}, SiO₂(2%)/TiO_{2_400} and SiO₂(4%)/TiO_{2_400}, (B) starting TiO_{2_400}, SiO₂(7.7%)/TiO_{2_400}, SiO₂(11.1%)/TiO_{2_400}, SiO₂(14.3%)/TiO_{2_400} and SiO₂(17.2%)/TiO_{2_400}.

Table 1 shows the specific surface area value and the pore size distribution for all the obtained materials. The specific surface area of the starting TiO_2 was $193 \text{ m}^2/\text{g}$. The values presented in Table 1 show that the photocatalysts modified with silica were characterized by a higher specific surface area (up to $234 \text{ m}^2/\text{g}$) in comparison to the materials obtained the same way but without the addition of SiO_2 . The average size of anatase crystallites has not changed. Therefore, the use of silica in the titanium dioxide modification process contributed to the increase in the specific surface area of the photocatalysts. The specific surface area of the silica used for modification was $>200 \text{ m}^2/\text{g}$ [44]. Bao et al. [45] also observed an increase in the surface area for the materials modified with silica. In this case, the specific surface area changed from $15.4 \text{ m}^2/\text{g}$ for pure TiO_2 to $127.7 \text{ m}^2/\text{g}$ for silica-modified TiO_2 . Table 1 noted that, as the SiO_2 content increased, the total pore volume also increased. This is a normal phenomenon associated with an increase in the size of a specific surface area. For example, the pore volume for the starting TiO_2 was $0.109 \text{ cm}^3/\text{g}$, and for $\text{SiO}_2(17.2\%)/\text{TiO}_2$ was $0.366 \text{ cm}^3/\text{g}$. It can be concluded that the SiO_2 modification had a significant effect on the increase in S_{BET} and the total pore volume. After the heat treatment, the specific surface area of the reference photocatalysts decreased from $193 \text{ m}^2/\text{g}$ for the starting TiO_2 sample to $54 \text{ m}^2/\text{g}$ for the sample calcined at $400 \text{ }^\circ\text{C}$ (starting TiO_2 _400). Thus, the correlation between calcination and the decrease in the size of the specific surface area is possible to observe. Calcining titanium dioxide causes the sintering and agglomeration of TiO_2 particles, which then results in a decrease in the size of the specific surface area [46]. It should also be noted that the specific surface area did not decrease in the range of materials after calcination. This is related to the relatively large specific surface area of silica and the fact that the addition of silica inhibits the growth of crystallites. The specific surface area of photocatalysts changed from $54 \text{ m}^2/\text{g}$ for the starting TiO_2 _400 to $146 \text{ m}^2/\text{g}$ for the $\text{SiO}_2(17.2\%)/\text{TiO}_2$ _400 sample.

Scanning electron microscope analysis in the SE (secondary electron) mode was conducted to determine the morphology of obtained photocatalysts and the approximate size of agglomerates/aggregates that form $\text{SiO}_2/\text{TiO}_2$ particles. Figure 5A–C shows example SEM images for the starting TiO_2 and the $\text{SiO}_2(14.3\%)/\text{TiO}_2$ _400 sample. The SEM images shown in Figure 5A,B indicate that the particles of starting TiO_2 form large aggregates consisting of finely agglomerated particles and larger clusters at the periphery, forming a matrix of large aggregates. An irregular and indeterminate shape characterized the individual particles. It is also worth noting that the TiO_2 particles were embedded in unreacted TTIP matrix. After the modification process using SiO_2 and calcination in an argon atmosphere, the grains had a more regular spherical shape. An increase in the size of photocatalyst aggregates was also observed after modification (350–500 nm) compared to the starting TiO_2 (150–350 nm). This results from the tendency of silica particles to form larger structures [47]. In addition, silica can effectively prevent the growth of TiO_2 crystallites after calcination, and it is well known that the tendency of particle agglomeration/aggregation is especially observed for small particles [38,39]. Both the starting TiO_2 and $\text{SiO}_2(14.3\%)/\text{TiO}_2$ _400 particles tended to form large aggregates. However, it can be noted that the aggregation ability of the photocatalyst particles increased due to the modification of titanium dioxide with silica.

In Figure 6A,B, the UV-Vis/DR spectra of starting TiO_2 , silica-modified TiO_2 and samples calcined in an argon atmosphere are shown. The $\text{SiO}_2/\text{TiO}_2$ materials exhibited typical absorption of radiation in the UV area due to the intrinsic absorption of TiO_2 [48]. For the starting TiO_2 _400 sample, an absorption peak was observed at 305 nm, which was related to the transition of an electron from the valence band (O 2p) to the conduction band (Ti 3d) [49]. Compared with the reference sample, all silica-modified materials showed a shift in the absorption edge toward lower wavelengths (blue shift). The values of the band gap energy of $\text{SiO}_2/\text{TiO}_2$ photocatalysts were higher than the starting TiO_2 because of the blue shift that occurred due to modification. According to the literature [45], the increase in the value of band gap energy can be attributed to the quantum effect. This increase in the value of band gap energy causes a decrease in the energy valence band and an increase in the edge of the conductivity band, which may lead to the slowdown of the electron–hole

pair recombination process. In turn, the slowing the electron–hole pair recombination process contributes to the increase in photocatalytic activity.

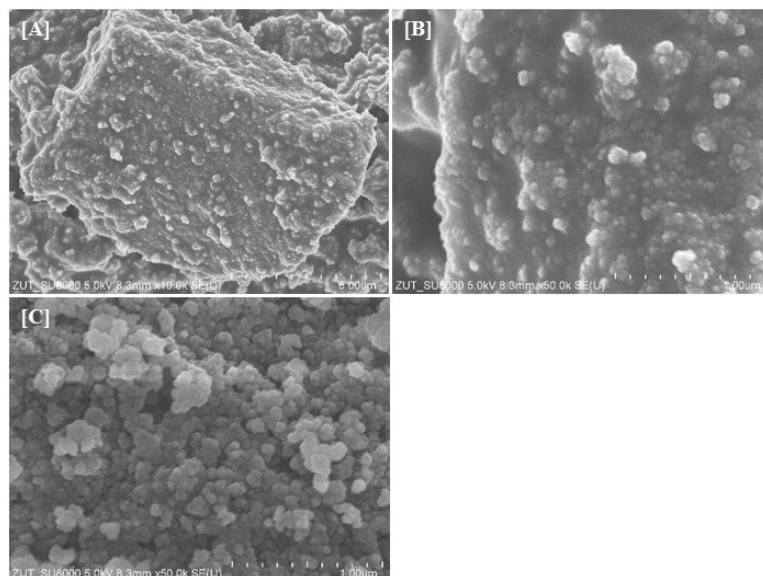


Figure 5. SEM images taken for (A,B) starting TiO_2 captured at different magnifications and (C) $\text{SiO}_2(14.3\%)/\text{TiO}_2\text{-400}$.

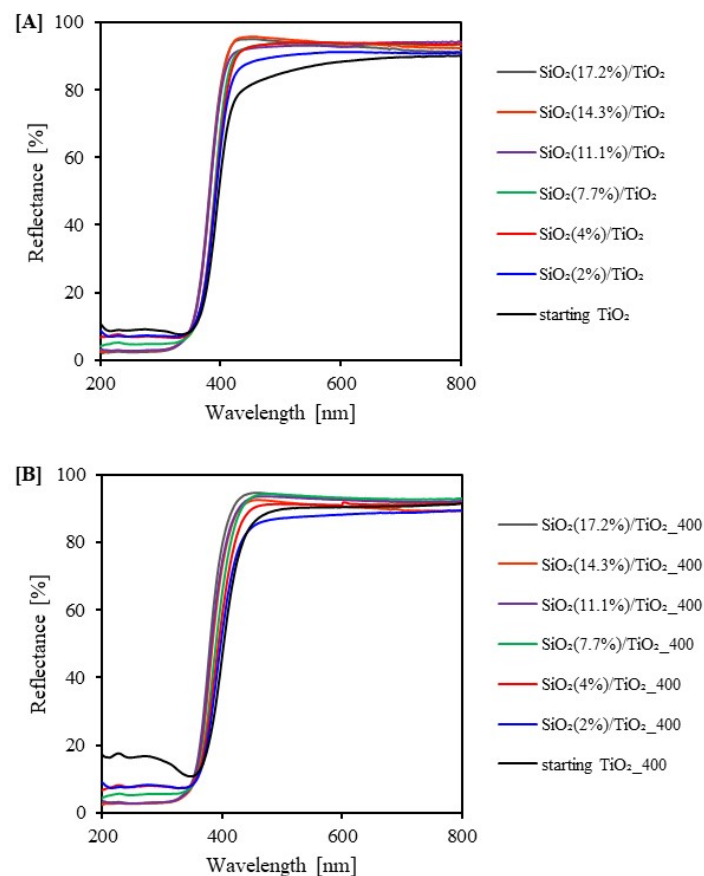


Figure 6. UV-Vis/DR spectra of starting TiO_2 and silica-modified TiO_2 prior (A) and after heat treatment (B).

According to the data presented in Table 2, silica modification did not change the surface character of the tested materials. After the modification, the surface of the $\text{SiO}_2/\text{TiO}_2$

photocatalysts remained positively charged, as did the surface of the reference sample without any SiO₂ content. Silicon-derived bands were observed on the FT-IR spectra of the studied samples. Ferreiry-Neto et al. [50] showed that modification of TiO₂ with silica causes a decrease in the zeta potential. Therefore, the TiO₂ photocatalysts modified with silica showed lower zeta potential values than the starting TiO₂. It is also important to note the decrease in zeta potential for SiO₂/TiO₂ photocatalysts after heating compared to non-calcined materials. Moreover, as the pH increased, the zeta potential value for these samples decreased. The higher the pH, the lower the zeta potential value of tested materials. The SiO₂(17.2%)/TiO₂_400 sample showed the lowest zeta potential (+14.6 mV). Our observations agree with those of Nowacka et al. [51], who found that the zeta potential decreases with increasing pH value, confirming that the zeta potential value strongly depends on pH.

Table 2. The band gap energy and zeta potential values of starting TiO₂ and silica-modified titania photocatalysts.

| Sample Code | E _g [eV] | pH | Zeta Potential δ [mV] |
|--|---------------------|-----|-----------------------|
| starting TiO ₂ | 3.05 ± 0.01 | 3.1 | +38.9 |
| SiO ₂ (2%)/TiO ₂ | 3.09 ± 0.01 | 2.8 | +35.8 |
| SiO ₂ (4%)/TiO ₂ | 3.10 ± 0.01 | 3.2 | +35.7 |
| SiO ₂ (7.7%)/TiO ₂ | 3.12 ± 0.01 | 3.2 | +32.8 |
| SiO ₂ (11.1%)/TiO ₂ | 3.22 ± 0.01 | 3.3 | +33.6 |
| SiO ₂ (14.3%)/TiO ₂ | 3.22 ± 0.01 | 3.4 | +31.0 |
| SiO ₂ (17.2%)/TiO ₂ | 3.23 ± 0.01 | 3.4 | +31.0 |
| starting TiO ₂ _400 | 2.98 ± 0.01 | 4.1 | +39.0 |
| SiO ₂ (2%)/TiO ₂ _400 | 3.07 ± 0.01 | 4.0 | +33.2 |
| SiO ₂ (4%)/TiO ₂ _400 | 3.11 ± 0.01 | 4.2 | +30.2 |
| SiO ₂ (7.7%)/TiO ₂ _400 | 3.15 ± 0.01 | 4.3 | +19.5 |
| SiO ₂ (11.1%)/TiO ₂ _400 | 3.23 ± 0.01 | 4.4 | +19.7 |
| SiO ₂ (14.3%)/TiO ₂ _400 | 3.22 ± 0.01 | 4.4 | +17.9 |
| SiO ₂ (17.2%)/TiO ₂ _400 | 3.24 ± 0.01 | 4.5 | +14.6 |

2.2. Photocatalytic Activity Test

The photocatalytic activity of the starting TiO₂ and the new silica-modified TiO₂ photocatalysts were assessed based on the methylene blue degradation under the influence of UV radiation. The photolysis of dye solution (without the addition of a photocatalyst, see Figure 7) was also investigated. The experiment showed that the MB decomposition due to the photolysis process was negligible (ca. 0.5%). The distribution of methylene blue in the presence of starting TiO₂ and TiO₂ modified with silica before and after heat treatment is shown in Figure 8A,B. In addition, the results of the dye decomposition rate after 5 h of UV (138 W/m² UV in the range of 280–400 nm and 167 W/m² VIS in the range of 300–2800 nm) irradiation were compared, as shown in Figure 9A,B. It should be noted that all SiO₂/TiO₂ photocatalysts showed higher activity compared to the photocatalyst without the addition of SiO₂. Undoubtedly, the amount of silica used for modification played an important role in the photoactivity of the tested samples. It was observed that the decomposition degree increased with an increase in the SiO₂ content in the sample (up to 14.3 wt.% of SiO₂). SiO₂(11.1%)/TiO₂ and SiO₂(14.3%)/TiO₂ samples demonstrated the highest activity, for which the methylene blue degradation degree was 40.99 and 42.73%, respectively. In comparison, the MB decomposition degree for the starting TiO₂ was 7.19%. The silica modification contributed to an increase in specific surface area and pore volume, as well as a change in the band gap energy value. All SiO₂-modified samples showed a higher specific surface area and pore volume than the starting TiO₂. For example, the specific surface area and pore volume of starting TiO₂ sample were 193 m²/g and 0.109 cm³/g, respectively, and those of the SiO₂(11.1%)/TiO₂ sample were 208 m²/g and 0.265 cm³/g. In addition, the use of silica in the titanium dioxide modification process contributed to the inhibition of S_{BET} decrease in the range of materials after calcination. For example, the size of specific surface

area for starting TiO₂_400 sample was 54 m²/g, while that for SiO₂(11.1%)/TiO₂_400 and SiO₂(14.3%)/TiO₂_400 was 121 m²/g and 135 m²/g, respectively. It is well known that the specific surface area has an important role in increasing photocatalytic activity [52]. The high surface area provides a number of active centers that can adsorb a large number of pollutant molecules [53]. In the case of post-calcination materials, a relationship between the increase in specific surface area and the increase in the applied silica weighting was also noted. The higher the amount of silica in the material composition, the higher the specific surface area. For example, the size of the specific surface area for the sample SiO₂(2%)/TiO₂_400 was 89 m²/g, and for the sample SiO₂(17.2%)/TiO₂_400, it was already 146 m²/g. This was related to the fact that silica inhibits the growth of crystallites. Another parameter influencing the improvement of the photocatalytic activity was the change in the band gap energy. The band gap energy for the SiO₂(11.1%)/TiO₂ and SiO₂(14.3%)/TiO₂ (3.22 eV) samples was higher than for the starting TiO₂ (3.05 eV). Moreover, a relationship between the increase in activity and the value of band gap energy was observed. The higher the value of band gap energy, the higher the activity. The highest activity was observed in photocatalysts, whose E_g value was 3.22 eV and 3.23 eV. Bao et al. [45] and Periyat et al. [54] suggested that the increase in band gap energy value slows down the electron–hole pair recombination process. This is since an increase in the band gap energy reduces the energy valence band and increases the edge of the conductivity band. The phase composition was also an important parameter determining the activity. It is important to note that the photocatalysts that showed the highest activity comprised 66–72% anatase and 28–34% brookite. Similar results were also obtained by Allen et al. [55], who studied the effect of the brookite phase on the photoactivity of TiO₂. They showed that photocatalysts mixtures of anatase and brookite show high photocatalytic activity. A photocatalyst obtained by calcination at 400 °C and containing 69% anatase and 31% brookite in its composition removed about 97% of methyl orange after 180 min of irradiation. This was explained by the fact that the conductivity band of the TiO₂ brookite phase is shifted more cathodically by 0.14 eV than that of anatase. This displacement facilitates interfacial electron transfer to molecular oxygen. It should be noted that photocatalysts after calcination showed higher activity compared to non-calcined materials. The higher activity for the samples after calcination was attributed to the larger crystallite size of anatase. The recorded increase in anatase crystallite size indicates the transformation of the amorphous phase present in non-calcined materials. Zhang et al. [56] determined that the photocatalytic activity is the highest when the anatase crystallite size is around 10 nm, which concord with our observations. In our case, the photocatalysts with a crystallite size up to 10 nm showed the highest activity.

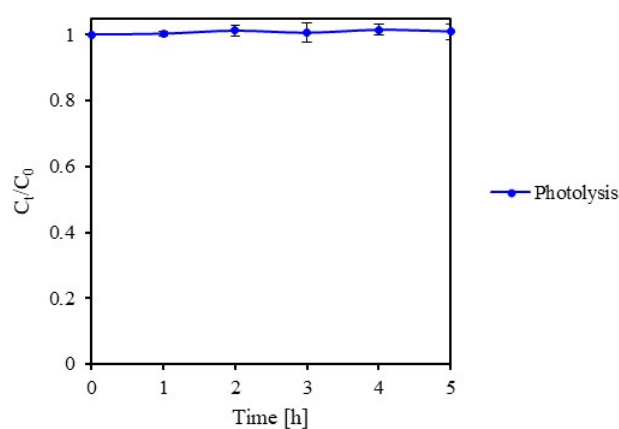


Figure 7. Methylene blue photolysis curve during 5 h of UV light irradiation.

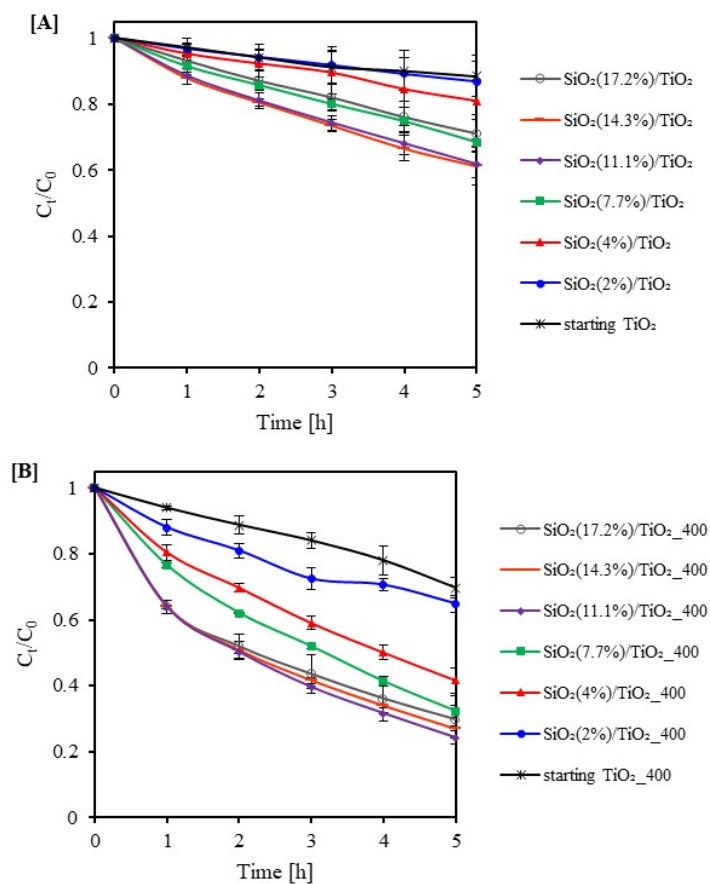


Figure 8. Methylene blue decomposition under UV irradiation of starting TiO_2 and silica-modified TiO_2 prior (A) and after calcination at 400 °C (B).

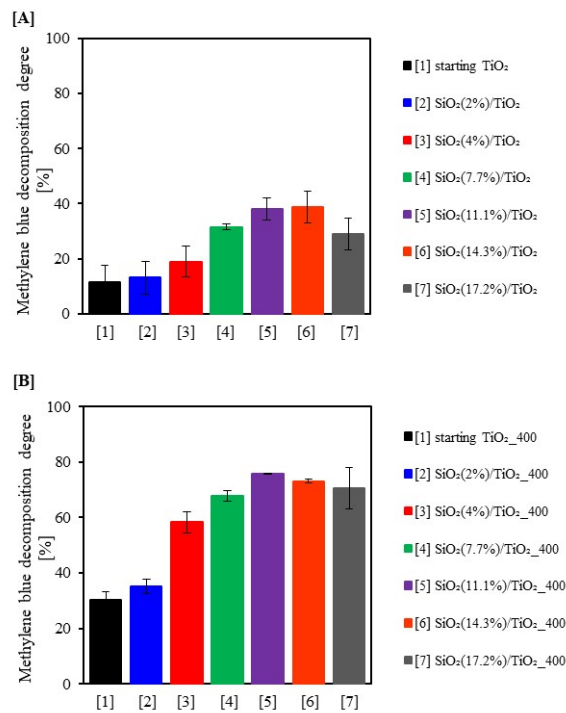


Figure 9. Methylene blue decomposition degree after 5 h of UV light irradiation for starting TiO_2 and silica-modified TiO_2 prior (A) and after calcination at 400 °C (B).

In order to better understand the photocatalytic degradation of methylene blue, the apparent reaction rate constants were determined. The degradation of methylene blue for the starting TiO_2 _400 followed the zero-order model. However, for $\text{SiO}_2(4\%)/\text{TiO}_2$, $\text{SiO}_2(7.7\%)/\text{TiO}_2$, $\text{SiO}_2(17.2\%)/\text{TiO}_2$, $\text{SiO}_2(4\%)/\text{TiO}_2$ _400, $\text{SiO}_2(7.7\%)/\text{TiO}_2$ _400 and $\text{SiO}_2(11.1\%)/\text{TiO}_2$ _400, the dye degradation followed a pseudo-first-order model. For all other samples, the degradation followed a pseudo-second-order model. The linear transformations of zero order, pseudo-first order, and pseudo-second order are shown in Figure 10A–C. It can be seen that, after 3 h of radiation, the points on the graphs started to deviate slightly from the typical linear curve. The observed reduction in reaction rate was due to the formation of intermediates during the dye decomposition. According to the data presented in Table 3, the highest k_1 values of methylene blue decomposition were obtained for the heat-treated photocatalysts. Similar to the pseudo-first-order model, higher k_2 values were recorded for the materials after calcination. It should be noted that the highest rate constant (0.052 L/(min·mg)) was observed for $\text{SiO}_2(14.3\%)/\text{TiO}_2$ _400, and this value is 17.3 times higher than for starting TiO_2 .

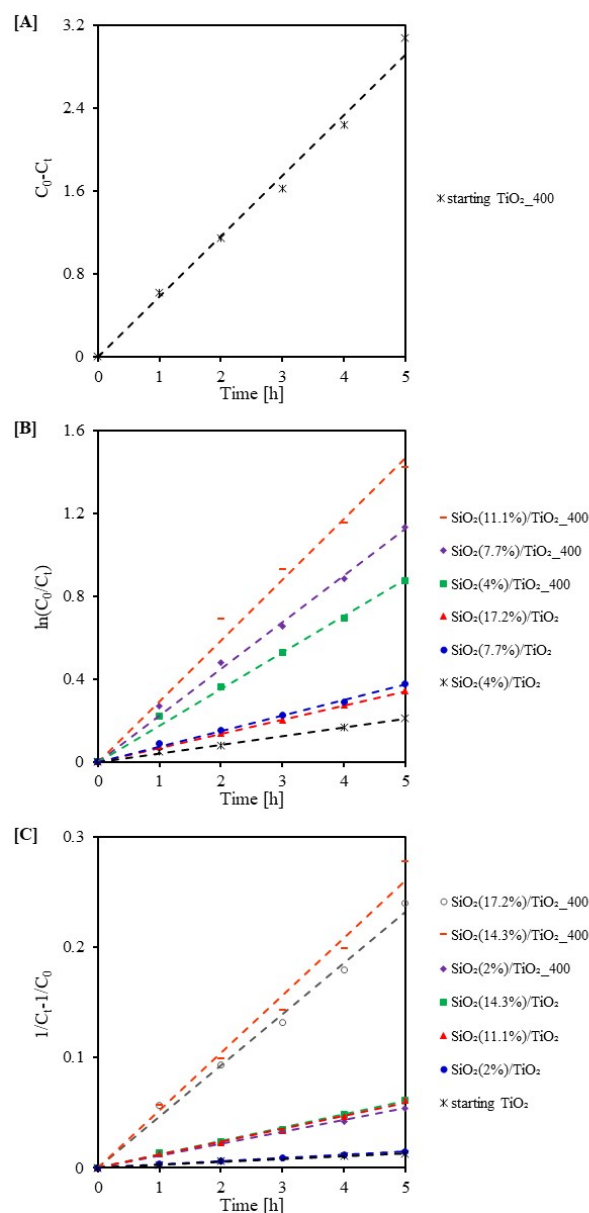


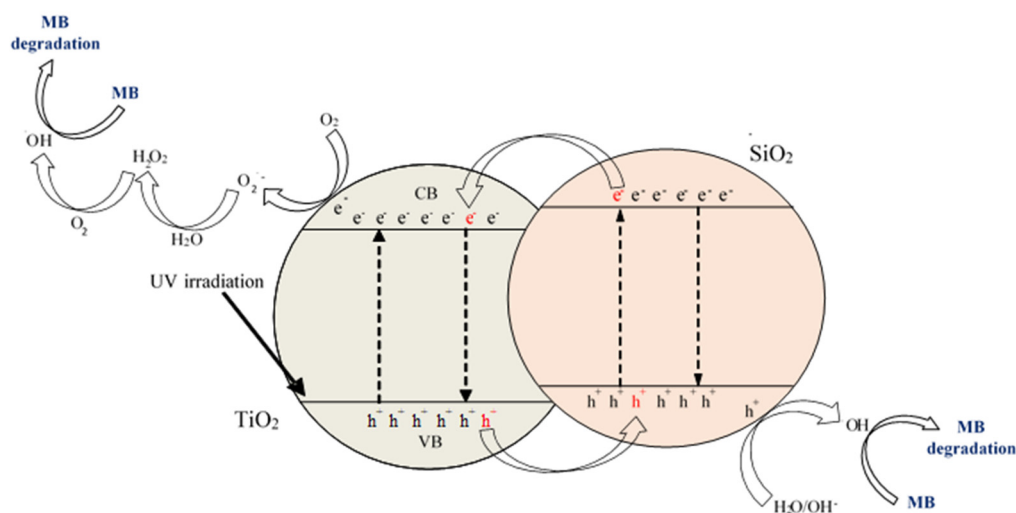
Figure 10. The zero-order plot (A), the pseudo-first-order (B), and the pseudo-second-order plot (C) of methylene blue decomposition.

Table 3. The fitting parameters, zero, pseudo-first, and pseudo-second reaction rate constants for methylene blue decomposition (after 5 h of UV radiation).

| Sample Code | k_0 (mg/(L·min)) | R^2 | Sample Code | k_1 (1/min) | R^2 | Sample Code | k_2 (L/(min·mg)) | R^2 |
|--------------------------------|-----------------------|-------|--|------------------|-------|--|-----------------------|-------|
| starting TiO ₂ _400 | 0.583 | 0.99 | SiO ₂ (4%)/TiO ₂ | 0.042 | 0.99 | starting TiO ₂ | 0.003 | 0.99 |
| | | | SiO ₂ (17.2%)/TiO ₂ | 0.068 | 0.99 | SiO ₂ (2%)/TiO ₂ | 0.003 | 0.99 |
| | | | SiO ₂ (7.7%)/TiO ₂ | 0.075 | 0.99 | SiO ₂ (2%)/TiO ₂ _400 | 0.011 | 0.99 |
| | | | SiO ₂ (4%)/TiO ₂ _400 | 0.176 | 0.99 | SiO ₂ (11.1%)/TiO ₂ | 0.012 | 0.99 |
| | | | SiO ₂ (7.7%)/TiO ₂ _400 | 0.225 | 0.99 | SiO ₂ (14.3%)/TiO ₂ | 0.012 | 0.99 |
| | | | SiO ₂ (11.1%)/TiO ₂ _400 | 0.294 | 0.98 | SiO ₂ (17.2%)/TiO ₂ _400 | 0.046 | 0.99 |
| | | | | | | SiO ₂ (14.3%)/TiO ₂ _400 | 0.052 | 0.98 |

2.3. Photocatalytic Mechanism

The proposed mechanism for methylene blue (MB) degradation in the presence of SiO₂/TiO₂ is shown in Figure 11. When the photocatalyst absorbs a photon with an energy equal or greater than the band gap energy, the activation occurs, which means an electron ejection from the valence band and its transfer to the conduction band with the generation of an electron gap. The active hydroxyl radicals are generated. As an active oxidizing agent, the hydroxyl radicals attack the MB presents at the surface of TiO₂ and decompose it into harmless species, such as carbon dioxide and water. However, it is well known that the high recombination of photogenerated e⁻-h⁺ pairs makes it difficult for the effective photodegradation of pollutants. According to the literature [57,58], connection between TiO₂ and SiO₂ (in our case, confirmed by the DRIFT analysis suggesting the presence of Ti–O–Si band) enhances charge carriers' separation (e⁻ and h⁺) and facilitates the transfer between each other. Thus, the suppression of the electron–hole recombination is limited, causing the enhancement in photoactivity.

**Figure 11.** Schematic of the photocatalysis mechanism on SiO₂/TiO₂ surface (based on [57]).

3. Materials and Methods

3.1. Materials and Reagents

The SiO₂/TiO₂ photocatalysts were obtained with the sol-gel method using titanium(IV) isopropoxide TTIP ($\geq 97\%$, Sigma-Aldrich Co., Saint Louis, MO, USA) as a precursor of TiO₂, fumed silica ($\geq 99.8\%$, $S_{BET} > 200$ m²/g, average particle size 7–14 nm, PlasmaChem GmbH, Germany) as a silica precursor, isopropyl alcohol (pure p.a, Firma Chempur[®], Piekary Śląskie, Poland) as a solvent and hydrochloric acid (35–38% pure, Firma Chempur[®], Piekary Śląskie, Poland) as a promoter of the hydrolysis reaction. Methyl-

lene blue (purity $\geq 82\%$, Firma Chempur[®], Piekary Śląskie, Poland) was used as an organic dye compound in photocatalytic tests.

3.2. Preparation of SiO₂/TiO₂ Photocatalysts

The sol-gel method was used to obtain SiO₂/TiO₂ photocatalysts. Titanium(IV) isopropoxide and fumed silica were chosen as TiO₂ and SiO₂ precursors, respectively. At first, 5 mL of titanium precursor was dropwise added to 15 mL of isopropyl alcohol. Then, 2, 4, 7.7, 11.1, 14.3, or 17.2 wt.% of silica precursor was added. Next, the pH of the obtained solution was adjusted to 2 with hydrochloric acid. Then, the hydrolysis process was started by slowly adding 100 mL of water: isopropyl alcohol mixture (25:75 *v/v*). In the end, the solution was placed in a magnetic stirrer for 1 h and then left for the ageing process taking 24 h. The obtained gel was dried in a muffle furnace at 100 °C for 24 h. Finally, the received material was calcined at 400 °C in a tube furnace under an argon atmosphere (60 mL/min, purity: 5.0, Messer Polska Sp. z o.o., Chorzów, Poland). The obtained photocatalysts were determined as follows: SiO₂(x%)/TiO₂_400, where x is the weight percentage of SiO₂ in the sample and 400 is the heating temperature. The reference sample, labelled as a starting TiO₂, was also received using the same method but without silica.

3.3. Characterization Methods

Diffuse reflectance DRIFT spectra were recorded using FT-IR-4200 spectrometer (JASCO International Co. Ltd., Tokyo, Japan) equipped with a DiffuseIR accessory (PIKE Technologies, Cottonwood Dr, Fitchburg, WI, USA) and were examined in the range of 4000–400 cm⁻¹. The crystalline structure of received photocatalysts was identified utilizing XRD analysis (Malvern PANalytical B.V., Almelo, The Netherlands), using Cu K α radiation ($\lambda = 0.154056$ nm). The XRD diffractograms were collected in the range of 20–80° on 2 θ scale. The PDF-4+ 2014 International Centre for Diffraction Data database (04-0028296 PDF4+ card for anatase and 04-007-0758 PDF4+ card for brookite) was used for the specification of the phase composition. The mean crystallite sizes of the nanomaterials were calculated using the Rietveld method. The surface area (S_{BET}) and pore volume of the tested photocatalysts were calculated from the nitrogen adsorption–desorption measurements at 77 K carried out in QUADRASORB evoTM Gas Sorption analyzer (Anton Paar GmbH, Graz, Austria). All samples were degassed at 100 °C for 16 h under a high vacuum before measurements to preclean the surface of the tested samples. The total pore volume (V_{total}) was calculated from the adsorbed nitrogen after the pore condensation was completed at a relative pressure $p/p_0 = 0.99$. The volume of micropores (V_{micro}) was determined using the Dubinin–Radushkevich equation. The volume of mesopores (V_{meso}) was determined as the difference between V_{total} and V_{micro} . The surface nature of the studied materials was determined from scanning electron microscopy SEM images. The SU8020 Ultra-High Resolution Field Emission microscope (Hitachi Ltd., Tokyo, Japan) was used for the measurements. The UV-Vis/DR diffuse reflection spectra of the prepared samples were recorded in the range of 200–800 nm using a V-650 UV-Vis spectrophotometer (JASCO International Co., Tokyo, Japan) equipped with an PIV-756 integrating sphere accessory for studying DR spectra. Spectralon (Spectralon[®] Diffuse Reflectance Material, Labsphere, USA) was used as the standard sample. The values of the band gap energy (E_g) of the studied photocatalysts were calculated with the Kubelk–Munk Equation (1) [59]:

$$F(R) = (1 - R)^2 / 2R \quad (1)$$

where

F(R)—radiation absorption coefficient;

R—reflectance.

From the above equation, the radiation absorption coefficient was determined. Next, the dependence of energy corresponding to each wavelength was plotted against the square of the inverse of the energy product and the absorption coefficient $(F(R) \cdot E)^{1/2}$.

Finally, a tangent was drawn where the fit is closest to the energy change curve. After transforming the equation of the plotted line, the value of band gap energy was obtained. ZetaSizer NanoSeries ZS (Malvern Panalytical Ltd., Malvern, UK) was used to determine the zeta potential values. The zero-order reaction rate constant can be described as (Equation (2)) [60]:

$$C_0 - C_t = k_0 t \quad (2)$$

The pseudo-first reaction rate constant was determined using the Langmuir–Hinshelwood kinetics model, as shown in Equation (3) [61]:

$$\ln(C_0/C_t) = kKt = k_1 t \quad (3)$$

While the pseudo-second reaction rate constant can be described as (Equation (4)) [62]:

$$1/C_t - 1/C_0 = k_2 t \quad (4)$$

where:

- C_0 —initial concentration of the methylene blue in solution [mg/L];
- C_t —concentration of the methylene blue at time t [mg/L];
- k_0 —zero-order reaction rate constant [mg/(L·min)];
- k_1 —pseudo-first reaction rate constant [1/min];
- k_2 —pseudo-second reaction rate constant [L/(min·mg)];
- t —time of irradiation [min];
- K —adsorption coefficient of the reactant [L/mg].

3.4. Photocatalytic Activity Test

The photocatalytic activity of the obtained SiO₂/TiO₂ materials was determined using a methylene blue (MB) solution (10 mg/L) as a model water pollutant. During the experiment, a glass beaker containing 0.2 g/L of the tested photocatalyst and 0.5 L of MB solution was placed under an artificial UV-VIS light source comprised of six lamps with the power of 20 W each (Philips) with the radiation intensity of about 138 W/m² UV (for the range of 280–400 nm) and 167 W/m² VIS (for the range of 300–2800 nm). The emission spectrum of the lamp used is shown in Figure 12. Prior to irradiation, the suspension was stirred in the dark for 1 h to establish the adsorption–desorption equilibrium. After that, the lamps were switched on, and the suspension was irradiated for 5 h while maintaining vigorous stirring. A sample (10 mL) of the suspension was collected every 1 h and then centrifuged to separate the photocatalyst from the MB solution to determine the MB degradation. The methylene blue absorbance was measured by the V-630 UV-Vis spectrometer (Jasco International Co., Tokyo, Japan). The degradation degree of methylene blue was described with C_t/C_0 formula, where C_t stands for the dye absorbance at a given time point and C_0 for the dye absorbance after adsorption.

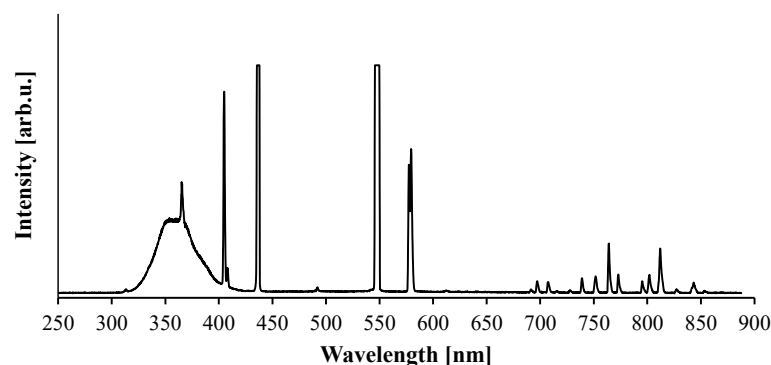


Figure 12. Emission spectrum of the UV-VIS lamp (6 × 20 W, Philips), 138 W/m² UV for 280–400 nm and 167 W/m² VIS for 300–2800 nm.

4. Conclusions

In conclusion, SiO₂/TiO₂ nanomaterials were prepared by a sol-gel method combined with a calcination process at 400 °C in an inert gas atmosphere. In this paper, fumed silica was used as a silica precursor for the first time. The presence of SiO₂ on the TiO₂ surface was confirmed by FT-IR/DRS infrared spectroscopy. The relationships between the effects of different properties on the photocatalytic activity of the obtained materials were determined. It was found that the modification with SiO₂ increased the specific surface area and total pore volume. In addition, the presence of a modifier contributed to a change in the value of band gap energy and effectively inhibited the growth of crystallites during thermal modification. The photoactivity of the obtained samples was investigated by the degradation of methylene blue under UV irradiation. In general, it was found that the applied modification of titanium dioxide using SiO₂, both without and with the calcination phase, contributed to the increase in photocatalytic activity. All the obtained photocatalysts showed higher activity (up to 75.81%) than the starting TiO₂, which removed only 7.19% of methylene blue. Moreover, the photocatalytic activity increased with increasing SiO₂ content in the sample. Samples containing 11.1 and 14.3 wt.% SiO₂ showed the highest removal of methylene blue.

Author Contributions: Conceptualization: A.B. and A.W.; investigation: A.B., A.W. and M.S.; data curation: A.W., E.K.-N. and A.W.M.; writing—original draft preparation: A.B.; writing—review and editing: A.W., E.K.-N. and A.W.M.; project administration: A.W.M.; funding acquisition: A.W.M. All authors have read and agreed to the published version of the manuscript.

Funding: This work was supported by grant 2017/27/B/ST8/02007 from the National Science Centre, Poland.

Data Availability Statement: The data presented in this study are available upon request from the corresponding author.

Conflicts of Interest: The authors declare no conflict of interest.

References

1. Liu, C.; Mao, S.; Wang, H.; Wu, Y.; Wang, F.; Xia, M.; Chen, Q. Peroxymonosulfate-assisted for facilitating photocatalytic degradation performance of 2D/2D WO₃/BiOBr S-scheme heterojunction. *Chem. Eng. J.* **2022**, *430*, 132806. [[CrossRef](#)]
2. Liu, C.; Mao, S.; Shi, M.; Wang, F.; Xia, M.; Chen, Q.; Ju, X. Peroxymonosulfate activation through 2D/2D Z-scheme CoAl-LDH/BiOBr photocatalyst under visible light for ciprofloxacin degradation. *J. Hazard. Mater.* **2021**, *420*, 126613. [[CrossRef](#)] [[PubMed](#)]
3. Liu, C.; Mao, S.; Shi, M.; Hong, X.; Wang, D.; Wang, F.; Xia, M.; Chen, Q. Enhanced photocatalytic degradation performance of BiVO₄/BiOBr through combining Fermi level alteration and oxygen defect engineering. *Chem. Eng. J.* **2022**, *449*, 137757. [[CrossRef](#)]
4. Boyjoo, Y.; Sun, H.; Liu, J.; Pareek, V.K.; Wang, S. A review on photocatalysis for air treatment: From catalyst development to reactor design. *Chem. Eng. J.* **2017**, *310*, 537–559. [[CrossRef](#)]
5. Reddy, P.V.L.; Kavitha, B.; Reddy, P.A.K.; Kim, K.H. TiO₂-based photocatalytic disinfection of microbes in aqueous media: A review. *Environ. Res.* **2017**, *154*, 296–303. [[CrossRef](#)]
6. Nyamukamba, P.; Okoh, O.; Mungondori, H.; Taziwa, R.; Zinya, S. Synthetic methods for titanium dioxide nanoparticles: A review. In *Titanium Dioxide—Material for a Sustainable Environment*; IntechOpen: London, UK, 2018. [[CrossRef](#)]
7. Chen, H.S.; Kumar, R.V. Sol-gel TiO₂ in self-organization process: Growth, ripening and sintering. *RSC Adv.* **2012**, *2*, 2294–2301. [[CrossRef](#)]
8. Badmus, K.O.; Wewers, F.; Al-Abri, M.; Shahbaaz, M.; Petrik, L.F. Synthesis of Oxygen Deficient TiO₂ for Improved Photocatalytic Efficiency in Solar Radiation. *Catalysts* **2021**, *11*, 904. [[CrossRef](#)]
9. Tsebriienko, T.; Popov, A.I. Effect of poly (titanium oxide) on the viscoelastic and thermophysical properties of interpenetrating polymer networks. *Crystals* **2021**, *11*, 794. [[CrossRef](#)]
10. Serga, V.; Burve, R.; Krumina, A.; Romanova, M.; Kotomin, E.A.; Popov, A.I. Extraction-pyrolytic method for TiO₂ polymorphs production. *Crystals* **2021**, *11*, 431. [[CrossRef](#)]
11. Jiang, Y.; Amal, R. Selective synthesis of TiO₂-based nanoparticles with highly active surface sites for gas-phase photocatalytic oxidation. *Appl. Catal. B Environ.* **2013**, *138*, 260–267. [[CrossRef](#)]
12. Danks, A.E.; Hall, S.R.; Schnepf, Z.J.M.H. The evolution of ‘sol-gel’ chemistry as a technique for materials synthesis. *Mater. Horiz.* **2016**, *3*, 91–112. [[CrossRef](#)]

13. Tryba, B.; Tygielska, M.; Colbeau-Justin, C.; Kusiak-Nejman, E.; Kapica-Kozar, J.; Wróbel, R.; Żołnierkiewicz, G.; Guskos, N. Influence of pH of sol-gel solution on phase composition and photocatalytic activity of TiO₂ under UV and visible light. *Mater. Res. Bull.* **2016**, *84*, 152–161. [[CrossRef](#)]
14. Ciesielczyk, F.; Przybysz, M.; Zdarta, J.; Piasecki, A.; Paukszta, D.; Jesionowski, T. The sol-gel approach as a method of synthesis of xMgO·ySiO₂ powder with defined physicochemical properties including crystalline structure. *J. Sol-Gel Sci. Technol.* **2014**, *71*, 501–513. [[CrossRef](#)]
15. Daghbir, R.; Drogui, P.; Robert, D. Modified TiO₂ for environmental photocatalytic applications: A review. *Ind. Eng. Chem. Res.* **2013**, *52*, 3581–3599. [[CrossRef](#)]
16. Pal, A.; Jana, T.K.; Chatterjee, K. Silica supported TiO₂ nanostructures for highly efficient photocatalytic application under visible light irradiation. *Mater. Res. Bull.* **2016**, *76*, 353–357. [[CrossRef](#)]
17. Raj, K.; Smith, Y.R.; Subramanian, V.R.; Viswanathan, B. Structural studies of silica modified titania and its photocatalytic activity of 4-chlorophenol oxidation in aqueous medium. *Indian J. Chem.* **2010**, *49*, 867–875.
18. Fu, X.; Clark, L.A.; Yang, Q.; Anderson, M.A. Enhanced photocatalytic performance of titania-based binary metal oxides: TiO₂/SiO₂ and TiO₂/ZrO₂. *Environ. Sci. Technol.* **1996**, *30*, 647–653. [[CrossRef](#)]
19. Jimmy, C.Y.; Yu, J.; Ho, W.; Zhao, J. Light-induced super-hydrophilicity and photocatalytic activity of mesoporous TiO₂ thin films. *J. Photochem. Photobiol. A Chem.* **2002**, *148*, 331–339.
20. Yu, J.; Zhao, X.; Jimmy, C.Y.; Zhong, G.; Han, J.; Zhao, Q. The grain size and surface hydroxyl content of super-hydrophilic TiO₂/SiO₂ composite nanometer thin films. *J. Mater. Sci. Lett.* **2001**, *20*, 1745–1748.
21. Chun, H.; Yizhong, W.; Hongxiao, T. Influence of adsorption on the photodegradation of various dyes using surface bond-conjugated TiO₂/SiO₂ photocatalyst. *Appl. Catal. B Environ.* **2001**, *35*, 95–105. [[CrossRef](#)]
22. Xie, C.; Xu, Z.; Yang, Q.; Xue, B.; Du, Y.; Zhang, J. Enhanced photocatalytic activity of titania-silica mixed oxide prepared via basic hydrolyzation. *Mater. Sci. Eng. S B* **2004**, *112*, 34–41. [[CrossRef](#)]
23. Ding, Z.; Lu, G.Q.; Greenfield, P.F. Role of the crystallite phase of TiO₂ in heterogeneous photocatalysis for phenol oxidation in water. *J. Phys. Chem. B* **2000**, *104*, 4815–4820. [[CrossRef](#)]
24. Fatimah, I. Preparation of TiO₂-SiO₂ via sol-gel method: Effect of silica precursor on catalytic and photocatalytic properties. In Proceedings of the 11th Joint Conference on Chemistry in Conjunction with the 4th Regional Biomaterials Scientific Meeting, Purwokerto, Indonesia, 15–16 September 2016. [[CrossRef](#)]
25. Qourzal, S.; Barka, N.; Tamimi, M.; Assabane, A.; Nounah, A.; Ihlal, A.; Ait-Ichou, Y. Sol-gel synthesis of TiO₂-SiO₂ photocatalyst for β-naphthol photodegradation. *Mater. Sci. Eng. C* **2009**, *29*, 1616–1620. [[CrossRef](#)]
26. Nandanwar, R.; Singh, P.; Syed, F.F.; Haque, F.Z. Preparation of TiO₂/SiO₂ nanocomposite with non-ionic surfactants via sol-gel process and their photocatalytic study. *Orient. J. Chem.* **2014**, *30*, 1577–1584. [[CrossRef](#)]
27. Morawski, A.W.; Kusiak-Nejman, E.; Wanag, A.; Kapica-Kozar, J.; Wróbel, R.J.; Ohtani, B.; Aksienionek, M.; Lipińska, L. Photocatalytic degradation of acetic acid in the presence of visible light-active TiO₂-reduced graphene oxide photocatalysts. *Catal. Today* **2017**, *280*, 108–113. [[CrossRef](#)]
28. Resende, S.F.; Nunes, E.H.M.; Houmard, M.; Vasconcelos, W.L. Simple sol-gel process to obtain silica-coated anatase particles with enhanced TiO₂-SiO₂ interfacial area. *J. Colloid Interface Sci.* **2014**, *433*, 211–217. [[CrossRef](#)]
29. Górska, P.; Zaleska, A.; Kowalska, E.; Klimczuk, T.; Sobczak, J.W.; Skwarek, E.; Janusz, W.; Hupka, J. TiO₂ photoactivity in vis and UV light: The influence of calcination temperature and surface properties. *Appl. Catal. B Environ.* **2008**, *84*, 440–447. [[CrossRef](#)]
30. Maira, A.J.; Coronado, J.M.; Augugliaro, V.; Yeung, K.L.; Conesa, J.C.; Soria, J. Fourier transform infrared study of the performance of nanostructured TiO₂ particles for the photocatalytic oxidation of gaseous toluene. *J. Catal.* **2001**, *202*, 413–420. [[CrossRef](#)]
31. Chesalov, Y.A.; Chernobay, G.B.; Andrushkevich, T.V. FTIR study of the surface complexes of β-picoline, 3-pyridine-carbaldehyde and nicotinic acid on sulfated TiO₂ (anatase). *J. Mol. Catal. A Chem.* **2013**, *373*, 96–107. [[CrossRef](#)]
32. Yang, G.; Jiang, Z.; Shi, H.; Xiao, T.; Yan, Z. Preparation of highly visible-light active N-doped TiO₂ photocatalyst. *J. Mater. Chem.* **2010**, *20*, 5301–5309. [[CrossRef](#)]
33. Araghi, M.A.; Shaban, N.; Bahar, M. Synthesis and characterization of nanocrystalline barium strontium titanate powder by a modified sol-gel processing. *Mater. Sci.-Pol.* **2016**, *34*, 63–68. [[CrossRef](#)]
34. Li, Z.; Hou, B.; Xu, Y.; Wu, D.; Sun, Y.; Hu, W.; Deng, F. Comparative study of sol-gel-hydrothermal and sol-gel synthesis of titania-silica composite nanoparticles. *J. Solid State Chem.* **2005**, *178*, 1395–1405. [[CrossRef](#)]
35. Andrade-Guel, M.; Díaz-Jiménez, L.; Cortés-Hernández, D.; Cabello-Alvarado, C.; Ávila-Orta, C.; Bartolo-Pérez, P.; Gamero-Melo, P. Microwave assisted sol-gel synthesis of titanium dioxide using hydrochloric and acetic acid as catalysts. *Boletín Soc. Española Cerámica Vidr.* **2019**, *58*, 171–177. [[CrossRef](#)]
36. Pelaez, M.; Nolan, N.T.; Pillai, S.C.; Seery, M.K.; Falaras, P.; Kontos, A.G.; Dunlop, P.S.M.; Hamilton, J.W.J.; Byrne, J.A.; O’Shea, K.; et al. A review on the visible light active titanium dioxide photocatalysts for environmental applications. *Appl. Catal. B Environ.* **2012**, *125*, 331–349. [[CrossRef](#)]
37. Kim, M.G.; Kang, J.M.; Lee, J.E.; Kim, K.S.; Kim, K.H.; Cho, M.; Lee, S.G. Effects of calcination temperature on the phase composition, photocatalytic degradation, and virucidal activities of TiO₂ nanoparticles. *ACS Omega* **2021**, *6*, 10668–10678. [[CrossRef](#)] [[PubMed](#)]
38. Xu, G.; Zheng, Z.; Wu, Y.; Feng, N. Effect of silica on the microstructure and photocatalytic properties of titania. *Ceram. Int.* **2009**, *35*, 1–5. [[CrossRef](#)]

39. Lu, Z.; Jiang, X.; Zhou, B.; Wu, X.; Lu, L. Study of effect annealing temperature on the structure, morphology and photocatalytic activity of Si doped TiO₂ thin films deposited by electron beam evaporation. *Appl. Surf. Sci.* **2011**, *257*, 10715–10720.
40. Sing, K.S.W. Reporting physisorption data for gas/solid systems with special reference to the determination of surface area and porosity (Provisional). *Pure Appl. Chem.* **1982**, *54*, 2201–2218. [[CrossRef](#)]
41. Sing, K.S.; Williams, R.T. Physisorption hysteresis loops and the characterization of nanoporous materials. *Adsorpt. Sci. Technol.* **2004**, *22*, 773–782.
42. Kutarov, V.V.; Tarasevich, Y.I.; Aksenenko, E.V.; Ivanova, Z.G. Adsorption hysteresis for a slit-like pore model. *Russ. J. Phys. Chem. A* **2011**, *85*, 1222–1227. [[CrossRef](#)]
43. Leofanti, G.; Padovan, M.; Tozzola, G.; Venturelli, B.J.C.T. Surface area and pore texture of catalysts. *Catal. Today* **1998**, *41*, 207–219. [[CrossRef](#)]
44. SiO₂—Krzemionka Koloidalna, Nanoproszek, Hydrofilowy. Available online: <https://3d-nano.com/pl/catalogue/sio2-krzemionka-koloidalna-nanoproszek-hydrofilowy/> (accessed on 22 September 2022).
45. Bao, N.; Wei, Z.; Ma, Z.; Liu, F.; Yin, G. Si-doped mesoporous TiO₂ continuous fibers: Preparation by centrifugal spinning and photocatalytic properties. *J. Hazard. Mater.* **2010**, *174*, 129–136. [[CrossRef](#)] [[PubMed](#)]
46. Nyamukamba, P.; Tichagwa, L.; Greyling, C. The influence of carbon doping on TiO₂ nanoparticle size, surface area, anatase to rutile phase transformation and photocatalytic activity. *Mater. Sci. Forum* **2012**, *712*, 49–63. [[CrossRef](#)]
47. Jesionowski, T.; Żurawska, J.; Krysztafkiewicz, A.; Pokora, M.; Waszak, D.; Tylus, W. Physicochemical and morphological properties of hydrated silicas precipitated following alkoxy silane surface modification. *Appl. Surf. Sci.* **2003**, *205*, 212–224. [[CrossRef](#)]
48. Tan, L.L.; Ong, W.J.; Chai, S.P.; Mohamed, A.R. Reduced graphene oxide-TiO₂ nanocomposite as a promising visible-light-active photocatalyst for the conversion of carbon dioxide. *Nanoscale Res. Lett.* **2013**, *8*, 465. [[CrossRef](#)]
49. Nilchi, A.; Janitabar-Darzi, S.; Mahjoub, A.R.; Rasouli-Garmarodi, S. New TiO₂/SiO₂ nanocomposites—Phase transformations and photocatalytic studies. *Colloids Surf. A: Physicochem. Eng. Asp.* **2010**, *361*, 25–30. [[CrossRef](#)]
50. Ferreira-Neto, E.P.; Ullah, S.; Simões, M.B.; Perissinotto, A.P.; de Vicente, F.S.; Noeske, P.L.M.; Ribeiro, S.J.L.; Rodrigues-Filho, U.P. Solvent-controlled deposition of titania on silica spheres for the preparation of SiO₂@TiO₂ core@shell nanoparticles with enhanced photocatalytic activity. *Colloids Surf. A Physicochem. Eng. Asp.* **2019**, *570*, 293–305. [[CrossRef](#)]
51. Nowacka, M.; Ambrożewicz, D.; Jesionowski, T. TiO₂-SiO₂/Ph-POSS functional hybrids: Preparation and characterisation. *J. Nanomater.* **2013**, *2013*, 1–10. [[CrossRef](#)]
52. Carp, O.; Huisman, C.L.; Reller, A. Photoinduced reactivity of titanium dioxide. *Prog. Solid State Chem.* **2004**, *32*, 33–177. [[CrossRef](#)]
53. Alvaro, M.; Aprile, C.; Benitez, M.; Carbonell, E.; García, H. Photocatalytic activity of structured mesoporous TiO₂ materials. *J. Phys. Chem. B* **2006**, *110*, 6661–6665. [[CrossRef](#)]
54. Periyat, P.; Baiju, K.V.; Mukundan, P.; Pillai, P.K.; Warriar, K.G.K. High temperature stable mesoporous anatase TiO₂ photocatalyst achieved by silica addition. *Appl. Catal. A Gen.* **2008**, *349*, 13–19. [[CrossRef](#)]
55. Allen, N.S.; Mahdjoub, N.; Vishnyakov, V.; Kelly, P.J.; Kriek, R.J. The effect of crystalline phase (anatase, brookite and rutile) and size on the photocatalytic activity of calcined polymorphic titanium dioxide (TiO₂). *Polym. Degrad. Stab.* **2018**, *150*, 31–36. [[CrossRef](#)]
56. Zhang, Z.; Wang, C.C.; Zakaria, R.; Ying, J.Y. Role of particle size in nanocrystalline TiO₂-based photocatalysts. *J. Phys. Chem. B* **1998**, *102*, 10871–10878. [[CrossRef](#)]
57. Nabih, S.; Shalan, A.E.; Serea, E.S.A.; Goda, M.A.; Sanad, M.F. Photocatalytic performance of TiO₂@SiO₂ nanocomposites for the treatment of different organic dyes. *J. Mater. Sci. Mater. Electron.* **2019**, *30*, 9623–9633. [[CrossRef](#)]
58. Gholami, T.; Bazarganipour, M.; Salavati-Niasari, M.; Bagheri, S. Photocatalytic degradation of methylene blue on TiO₂@SiO₂ core/shell nanoparticles: Synthesis and characterization. *J. Mater. Sci. Mater. Electron.* **2015**, *26*, 6170–6177. [[CrossRef](#)]
59. Chen, D.; Zou, L.; Li, S.; Zheng, F. Nanospherical like reduced graphene oxide decorated TiO₂ nanoparticles: An advanced catalyst for the hydrogen evolution reaction. *Sci. Rep.* **2016**, *6*, 20335. [[CrossRef](#)]
60. Abdullah, M.A.; Chong, F.K. Dual-effects of adsorption and photodegradation of methylene blue by tungsten-loaded titanium dioxide. *Chem. Eng. J.* **2010**, *158*, 418–425.
61. Sahoo, C.; Gupta, A.K.; Sasidharan Pillai, I.M. Photocatalytic degradation of methylene blue dye from aqueous solution using silver ion-doped TiO₂ and its application to the degradation of real textile wastewater. *J. Environ. Sci. Health* **2012**, *47*, 1428–1438. [[CrossRef](#)]
62. Khan, F.; Wahab, R.; Hagar, M.; Alnoman, R.; Rashid, M. Nanotransition materials (NTMs): Photocatalysis, validated high effective sorbent models study for organic dye degradation and precise mathematical data's at standardized level. *Nanomaterials* **2018**, *8*, 134. [[CrossRef](#)]